

## D. REACTION DYNAMICS

Over the last few years studies of various aspects of reaction dynamics using heavy-ion beams within the Division have steadily moved from measurements performed with ATLAS beams in the vicinity of the Coulomb Barrier towards higher beam energies. At present, the measurements at ATLAS focus mainly on reactions with exotic beams and on studies involving gamma-ray detection with Gammasphere: these are discussed elsewhere in this report. In addition to one contribution on inelastic scattering studies performed at ATLAS, this section presents work being performed at relativistic energies; i.e. the analysis of the AGS E917 experiment and the preparations for the PHOBOS experiment at RHIC.

### d.1. Angular Correlation, Spin Alignment, and Resonance Behavior in $^{12}\text{C}(^{12}\text{C}, ^{12}\text{C}) ^{12}\text{C}(3^-)$ Inelastic Scattering (A. H. Wuosmaa, B. B. Back, R. R. Betts, D. J. Blumenthal, S. Fischer, B. G. Glagola, D. J. Henderson, D. Hofman, R. V. F. Janssens, C. J. Lister, V. Nanal, D. Nisius, M. D. Rhein, P. R. Wilt, and M. Freer\*)

Many previous studies of inelastic scattering in the  $^{12}\text{C} + ^{12}\text{C}$  system have revealed strong resonance-like behavior. Several theoretical pictures have emerged which attempt to describe this behavior, either as super-deformed cluster states in the compound system  $^{24}\text{Mg}$ , or as potential scattering resonances whose strength is enhanced due to favorable angular momentum coupling conditions at particular energies. These models make predictions about the angular momenta expected to dominate the scattering process at resonance energies. Many of the reaction channels in which the strongest resonances are observed have non-zero channel spin, making the extraction of a resonance angular momentum difficult, if not impossible, using the traditional technique of angular distribution measurements. If, however, the radiation from the decay of the level in the inelastically excited nucleus can be detected, the angular correlations between that radiation, and the scattered nucleus, becomes sensitive to the total angular momentum of the system and, hence, the resonance spin. Furthermore, such angular

correlations may be used to study the alignment of the spin of the excited, scattered partner. Such data can provide information about the inelastic scattering process.

We have used these techniques to study features in the excitation functions of inelastic scattering in the  $^{12}\text{C} + ^{12}\text{C}$  system to the  $3^-$  state at 9.64 MeV in  $^{12}\text{C}$ , which decays to the alpha-particle unbound ground state of  $^8\text{Be}$ . Reilly *et al.*<sup>1</sup> and Fulton *et al.*<sup>2</sup> have reported the excitation function for this channel.<sup>1</sup> The three alpha particles from the decay of this level in  $^{12}\text{C}$  were detected in an array of double-sided silicon strip detectors (DSSDs). The data were sorted in order to extract the scattering yield as a function of the  $^{12}\text{C} + ^{12}\text{C}$  scattering angle, as well as the angle between the direction of the  $^8\text{Be}$  relative velocity and the beam direction. These correlated angular distributions, or angular correlations, were studied in order to learn about the reaction mechanism and to attempt to extract the spins of resonances in this channel. Some of the results of this work have appeared elsewhere.<sup>3</sup>

\*University of Birmingham, United Kingdom

<sup>1</sup>W. Reilly *et al.*, *Nuovo Cimento* **13A**, 913 (1973).

<sup>2</sup>B. R. Fulton *et al.*, *Phys. Rev. C* **21**, 198 (1980).

<sup>3</sup>A. H. Wuosmaa *et al.*, *Phys. Rev. C* **54**, 2463 (1996).

<sup>4</sup>Y. Kondo, Y. Abe, and T. Matsuse, *Phys. Rev. C* **19**, 1356 (1980).

<sup>5</sup>S. Marsh and W. D. M. Rae, *Phys. Lett.* **B153**, 21 (1985).

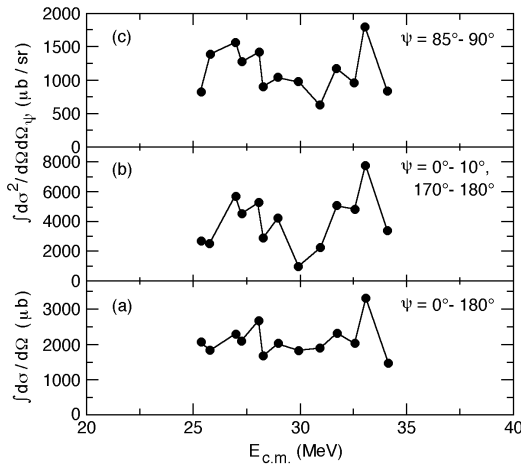


Fig. I-57. Excitation function for  $^{12}\text{C} + ^{12}\text{C}(3^-)$  inelastic scattering, for events with the angle between the  $\alpha$ - $^8\text{Be}$  relative velocity and the beam direction of (a) all values between  $0^\circ$  and  $180^\circ$  (b)  $0^\circ$ - $10^\circ$  and  $170^\circ$ - $180^\circ$ , and (c)  $85^\circ$ - $95^\circ$ .

A model-independent analysis of the angular correlation data may be obtained for events in which the alpha particle from the  $^{12}\text{C}(3^-)$  decay is detected at  $0^\circ$  with respect to a particular quantization axis, here chosen to lie along the beam direction. In this case, as there is no projection of the total angular momentum along the beam direction, the only magnetic substate which can contribute to the scattering is that with  $m = 0$ . Figure I-57 shows excitation function data for the  $3^-$  inelastic channel for the total cross section integrated from  $\text{C.M.} = 40^\circ$ - $105^\circ$  degrees in the lab and for the primary alpha particle detected at (a) all angles between  $0^\circ$  and  $180^\circ$ , (b)  $0^\circ$ - $10^\circ$  and  $170^\circ$ - $180^\circ$ , and (c)  $85^\circ$ - $95^\circ$ . The data in (b) and (c) correspond to scattering to the  $m = 0$ , and predominantly  $m = 1$  substates, respectively. The  $m = 0$  cross section shows the most significant variation in the cross section, with a peak-to-background ratio nearly a factor of two larger than that seen in (c). Such behavior is an indication that at the resonance energies, the spin of the  $3^-$  state

aligns predominantly perpendicular to the quantization axis, i.e. the assumption of a fully aligned system with the total angular momentum  $J = L + S$ , where  $L$  is the orbital angular momentum and  $S$  is the spin of the excited  $^{12}\text{C}$  state, the magnetic sub-state populations are expected to be approximately proportional to the Clebsch-Gordan coefficients  $|\langle L3\text{-mm}|J0\rangle|^2$ . Taking into account the solid angle  $\Delta\Omega$  for each bite in the alpha-particle correlation angle  $\psi$ , one expects the ratio of  $(\psi = 0^\circ + 180^\circ) / (\psi = 90^\circ)$  to be approximately 2, close to that which is observed in Fig. I-57.

Figure I-58 shows inelastic scattering angular distribution data for the  $m = 0$  substate obtained at several energies between 25 and 34 MeV. The solid curves represent Legendre polynomial partial-wave fits with three partial waves,  $L = 11, 13,$  and  $15$ . The dashed curves correspond to pure squared Legendre polynomials of order 13, at  $E_{\text{C.M.}} = 27.0$  MeV, and 15, at  $E_{\text{C.M.}} = 33.1$  MeV. These energies correspond to resonances reported by Fulton *et al.* Figure I-59 shows the energy dependence of the extracted partial cross sections  $\sigma_L$ . The enhancements in  $\sigma_{13}$  at 27 MeV, and  $\sigma_{15}$  at 33 MeV are clear, and consistent with the expectations from visual inspection of the  $m = 0$  angular distributions and comparison to the Legendre polynomial curves in Fig. I-59. These results confirm that the dominant orbital angular momenta are 13, and 15, for  $E_{\text{C.M.}} = 27$  and 33 MeV, respectively, and this information, combined with the observed alignment of the spin are consistent with spin assignments of  $J = 16^+$  and  $18^+$  for the two resonances, respectively, two units of angular momentum higher than those predicted by the band crossing model.<sup>4</sup> Finally, the spacing between the resonances is consistent with that expected for that between two rotational states with moments of inertia similar to that of two touching spheres, or of an extended deformed configuration resembling two orbiting  $^{12}\text{C}$  nuclei.<sup>5</sup>

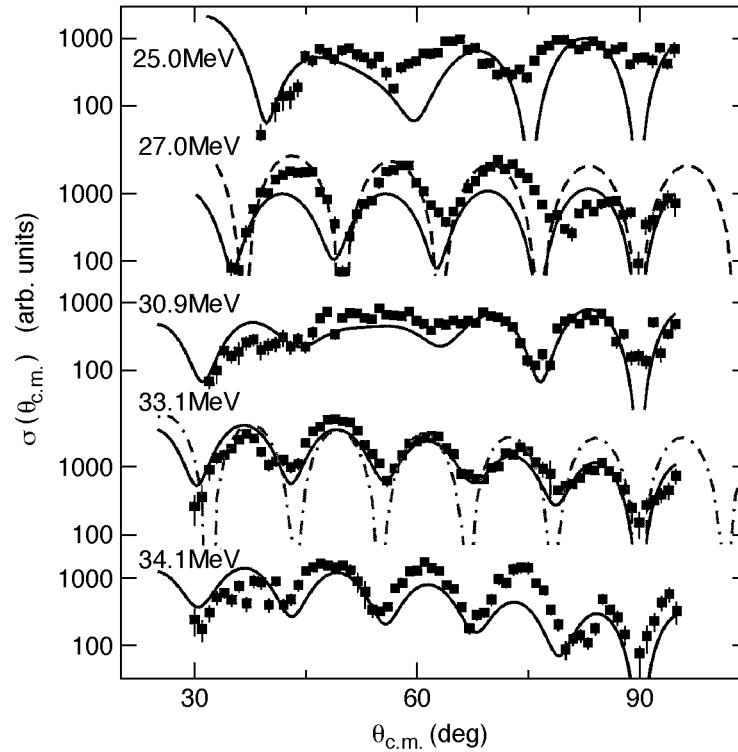


Fig. I-58.  $^{12}\text{C} + ^{12}\text{C}(3^-)$   $m = 0$  angular distribution data for several bombarding energies. The solid curves represent the Legendre-polynomial fits described in the text. The dashed, and dashed dotted curves represent pure squared Legendre polynomials of order 13, and 15 respectively.

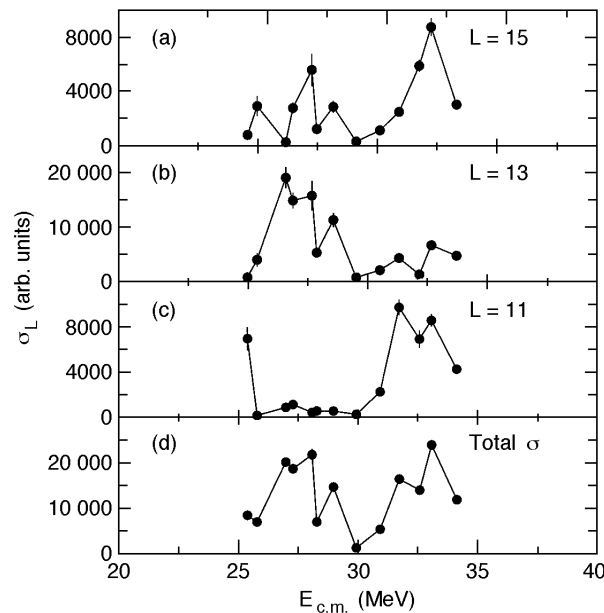


Fig. I-59. Energy dependence for partial wave cross sections  $\sigma_L$ , where  $L = 11$  (a), 13 (b) and 15 (c), and  $\Sigma_L(\sigma_L)$  (d), from Legendre-polynomial fits to the  $m = 0$  angular distributions.

## d.2. Studies of Au + Au Collisions at 6, 8, 10.8 GeV/Nucleon at the AGS

(E917 collaboration: B. B. Back, R. R. Betts,§ D. J. Hofman, V. Nanal, A. Wuosmaa, W. C. Chang,‡ C. Y. Chi,§§ Y. Y. Chu,† J. B. Cumming,† J. C. Dunlop,\*\*\* W. Eldredge,‡ S. Y. Fung,‡ R. Ganz,‡‡‡ E. J. Garcia-Solis,†† A. Gillitzer,¶¶ G. Heintzelman,† W. F. Henning,††† B. Holzman,§ J. H. Kang,†† E. J. Kim,\*\* S. Y. Kim,\*\* Y. Kwon,\*\* D. McLeod,§ A. C. Mignerey,†† M. Moulson,§§ C. A. Ogilvie,¶ R. Pak,‡‡ A. Ruangma,†† D. E. Russ,†† R. Seto,‡ P. J. Stankas,†† G. S. F. Stephans,¶ H. Q. Wang,‡ F. Wolfs,‡‡ H. Xiang,‡ G. Xu,‡ H. B. Yao,¶ and C. Zou‡)

### Introduction

Nuclear matter is compressed to high baryonic density in central collisions of heavy nuclei at relativistic energies. This opens the possibility of generating a new state of matter, the Quark-Gluon Plasma (QGP), in which quarks are not confined to baryons and mesons as is the case for normal matter. The question of whether sufficient densities can be achieved to generate the QGP at the beam energies available at the AGS accelerator at Brookhaven National Laboratory hinges critically on the degree of "stopping" that can be achieved, i.e. the pile-up of a large number of nucleons within a small interaction volume. Although it may be virtually impossible to study the instantaneous state of the interaction region, since the particles that are finally observed in the detectors may have undergone severe rescattering and/or coalescence processes during the later stages of the reaction, such information may still be embedded in the final distribution of particles.

In the E917 experiment at the AGS we have measured the spectra of protons, deuterons, pions, kaons,  $\eta$ 's, and  $\omega$ -mesons as well as some of their anti-particles emitted from the interaction volume and analyzed both their transverse and longitudinal components.

The collision dynamics was studied further by the way of the emission pattern relative to the reaction plane and by means of Hanbury-Brown Twiss analysis of two-particle correlations.

The E917 collaboration is now in its final phase of data analysis and the main results are presently being prepared for publications. Many preliminary results have been presented at various conferences, and included in conference proceedings.

### Experiment

The experimental arrangement is shown in Fig. I-60. It consists of a magnetic spectrometer which allows for momentum analysis of particles emerging from the target. Particle trajectories are tracked by several multiwire ionization chambers located both in front and behind the magnet. The time-of-flight wall provides particle identification when combined with the measured particle momentum.

Several beam counters located upstream of the target provide timing and trajectory information on each beam particle. When combined with the spatial location of the projectile remnant at the Hodoscope it is possible to determine the orientation of the reaction plane, with reasonable accuracy. The centrality of the collision (impact parameter) is obtained either by observing the multiplicity of particles (mostly pions) in the New Multiplicity Array (NMA) or the total energy of the projectile remnant in the Zero Degree Calorimeter ( $Z_{cal}$ ).

### Proton Spectra - Stopping

Proton spectra vs. transverse mass,  $m_t$ , have been measured over a wide range of rapidity and centrality. Each  $m_t$ -spectrum has been fit by a Boltzmann distribution in order to extrapolate into large  $m_t$  regions. The resulting integrated yields  $dN/dy$  for 5% most central collisions are shown as solid points in Fig. I-61(a-c); open points represent measured points reflected about mid-rapidity. Panels 4d-f shows the corresponding inverse slopes of the  $m_t$  spectra,  $T(y)$ . All data points are shown as a function of rapidity,  $y-y_{cm}$ , relative to the center-of-mass system. The  $dN/dy$  and inverse

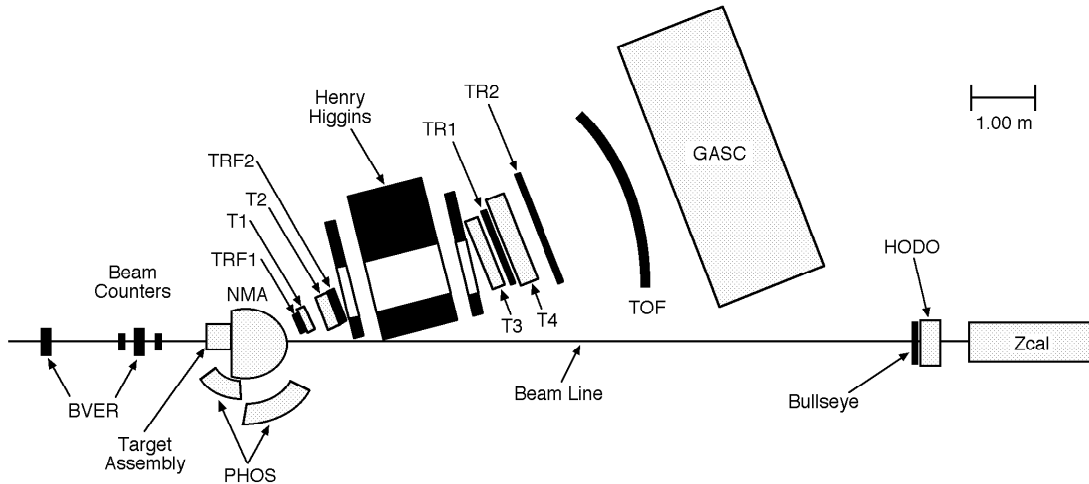


Fig. I-60. Experimental setup. See text for details.

slope data have been fit with a simple model, resulting in the solid curves. In this model the measured protons are assumed to be emitted isotropically from a continuous distribution of sources, which are uniformly distributed over a

rapidity range from  $-y_b - y_{cm}$  to  $y_b - y_{cm}$ . However, in order to simultaneously reproduce the data for the effective temperature, Fig. I-61(d-f), it was necessary to assume that the source temperature decreases with rapidity away from  $y_{cm}$  following

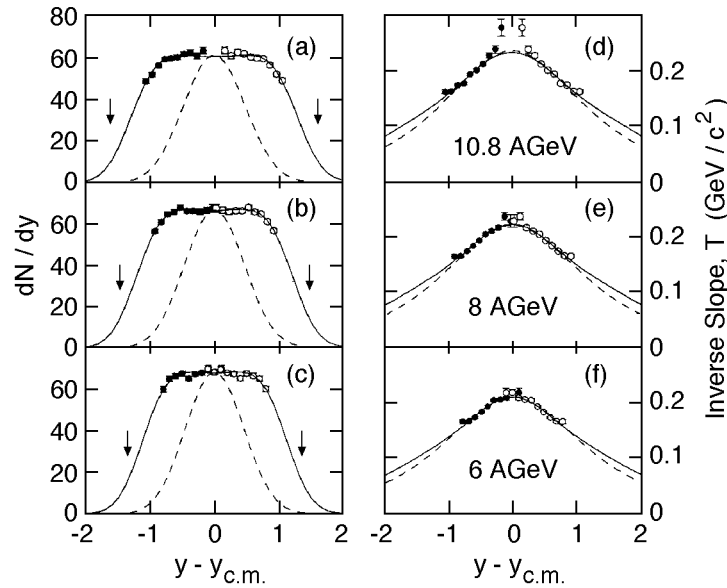


Fig. I-61. Measured (solid points) reflected (open circles) proton rapidity distributions and inverse slopes are shown as a function of rapidity  $y - y_{cm}$  for beam energies of 6, 8, and 10.8 GeV nucleon. The arrows indicate the target and beam rapidities. The dashed curves represent the expected distribution for isotropic emission from a thermal source at rest in the center-of-mass system ( $y = y_{cm}$ ), whereas the solid curves correspond to an optimum fit to the data for a uniform distribution of sources within a range of rapidities  $(y_{cm} - y_b) < (y_{cm} + y_b)$  with a Gaussian profile of  $T_{eff}(y)$  centered at  $y_{cm}$  (see text). The parameters obtained from a least squares fit to the data are  $y_b = 0.990, 1.086, 1.166$ ,  $\Upsilon_{eff}^0 = 0.253, 0.267, 0.279$  GeV/c<sup>2</sup> and  $\sigma_T = 0.697, 0.762, 0.809$  for  $E_{beam} = 6, 8, 10.8$  GeV/nucleon, respectively.

a Gaussian profile. We observe that this crude model is capable of reproducing the data very well, despite the fact that its basic assumptions are probably flawed. Thus it is generally accepted that the transverse  $m_t$  spectra is a result of both thermal and radial collective motion. However, in this analysis the fitted curves serve only to provide a reasonable extrapolation into the unmeasured region, which is required in order to obtain a standard measure of the degree of "stopping" in the process, namely the mean rapidity loss,  $\langle y \rangle$  of the projectile/target protons. The results are listed in Table 1 for the present data as well as Pb + Pb collisions at 158 GeV/nucleon from the CERN SPS program (NA49 collaboration). We observe that the absolute mean rapidity loss  $\langle y \rangle$  increases with beam energy (projectile rapidity). However, it is interesting to note that when the mean rapidity loss is normalized to the maximum possible rapidity loss,  $y^{\max} = y_{\text{beam}}/2$ , there is only a slight increase with beam energy.

To further evaluate the degree of "stopping" we have estimated the maximum fraction of the observed protons which can originate from an isotropically emitting source at rest in the c.m. system. The emission pattern from such a source is represented by the dashed curves in Fig. I-61. We first observe that the measured longitudinal distributions [Fig. I-61(a-c)] are significantly wider than expected for a thermal source in the c.m. system indicating a substantial degree of "transparency" in the collision. In one interpretation, this observation indicates that the only a relatively small fraction,  $f_{\text{iso}}$ , Table 1, of the incoming beam energy is converted to heat and particle production in the interaction region. Exactly how this translates to estimates of the maximum baryon density achieved in the collision does not follow directly and must be determined on the basis more realistic model calculations. This topic is discussed in further detail in Refs. 1-2.

Table 1. Measures of stopping in central heavy-ion collisions

$E_{\text{beam}}$ (A*GeV)	$\langle y \rangle$	$\langle y \rangle / y^{\max}$	$f_{\text{iso}}$
6.0	$0.74 \pm 0.01$	$0.55 \pm 0.01$	$0.49 \pm 0.01$
8.0	$0.82 \pm 0.01$	$0.56 \pm 0.01$	$0.46 \pm 0.01$
10.8	$0.93 \pm 0.01$	$0.57 \pm 0.01$	$0.45 \pm 0.01$
158	$1.68 \pm 0.01$	$0.58 \pm 0.01$	$0.23 \pm 0.02$

### Pion and Kaon Spectra

The pion and kaon production measured at 6 and 8 GeV/nucleon in the E917 experiment have been augmented with measurements at 2, 4, and 10.7 GeV/nucleon obtained in the predecessor

experiment E866 to obtain a rather complete excitation function.

As expected, we find that both  $K^+$  and  $K^0$  production, i.e. the rapidity density  $dN/dy$  at mid-

†Brookhaven National Laboratory, ‡University of California at Riverside, §University of Illinois at Chicago, ¶Massachusetts Institute of Technology, \*\*Yonsei University, Seoul, Korea, ††University of Maryland, ‡‡University of Rochester, §§Columbia University, ¶¶Forschungszentrum Julich, Germany, \*\*\*Yale University, †††GSI, Germany, ‡‡‡MPI, Germany

<sup>1</sup>Advances in Nuclear Dynamics 5, Plenum

Publishers, New York 1999, Eds. Bauer and Westfall, p. 131.

<sup>2</sup>B. B. Back *et al.*, submitted to Phys. Rev. Lett. (Feb. 2000).

rapidity  $y = y_{cm}$  increases drastically with beam energy as illustrated Fig. I-62. On the other hand, the mean transverse mass of the  $K^+$  and  $\pi^+$  spectra increase by less than 75% over the same beam energy range indicating that most of the increase in beam energy is converted to particle production.

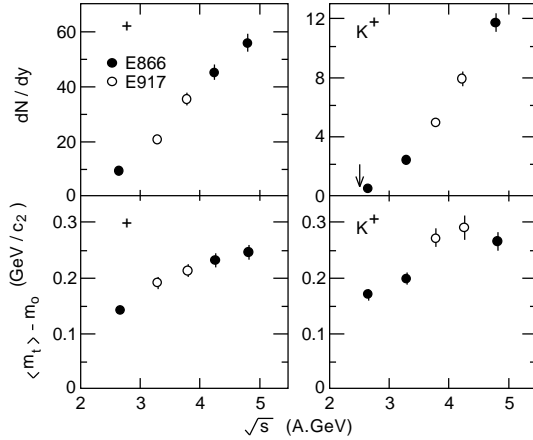


Fig. I-62. The yield of  $\pi^+$  and  $K^+$  at mid-rapidity (top panels) for central Au + Au reactions as a function of the initial available beam energy. The data from E866 are shown in filled circles and the data from E917 are shown as open circles. The lower panels show the mean  $m_{T, \perp}$  minus the rest mass for  $\pi^+$  and  $K^+$  at the same rapidity. The errors include both statistical and a 5% ( $dN/dy$ ), 5% (mean  $m_{T, \perp}$ ) point-to-point systematic uncertainty. The arrow indicates the threshold energy for producing  $K^+$  in a  $p + p$  reaction.

By comparing the ratio of  $K^+$  to  $\pi^+$  at mid rapidity we find, however, a substantially stronger, but smooth increase in strangeness production ( $K^+$ ) than expected from pure  $p + p$  collisions shown as circular points and the hatched area in Fig. I-63, respectively. This enhancement of strangeness production in nucleus-nucleus collisions is thought to arise from hadronic re-scattering processes within the hot interaction volume. There is, however, no experimental evidence for a sudden increase in strangeness production with beam energy, which has been suggested as a possible signal for the phase transition from hadronic matter

to the quark-gluon plasma. A manuscript presenting this analysis has been accepted for publication in Physics Lett. B.<sup>3</sup>

It has been predicted that mass of  $K^+$  and  $K^-$  may be modified in a dense medium, such as the one encountered in relativistic nucleus-nucleus collisions. This effect arises from the difference in the interaction between the two kaon species and the hadronic medium. Thus it is known that the mean-field interaction of  $K^-$  with baryons is attractive, whereas  $K^+$  interaction is repulsive. We have therefore studied the differences in  $K^+$  and  $K^-$  production with beam energy, which is expected to increase the density of the medium. In Fig. I-64 we show the ratio of rapidity density at mid-rapidity for  $K^-$  and  $K^+$  production as a function of c.m. energy  $\sqrt{s}$ . The kaon production thresholds in  $p + p$  collisions at  $s^{1/2} = 2.548$  GeV for  $K^+$  and  $s^{1/2} = 2.864$  GeV for  $K^-$  are indicated by the arrows. It is clear that the difference in phase space for the two production mechanisms has a strong effect also in heavy-ion collisions, although the production of both  $K^-$  and  $K^+$  extend well into the sub-threshold region. However, when the data are plotted as a function of energy relative to the production threshold  $s^{1/2} - s_{th}^{1/2}$  we find a distinctly different behavior above and below the threshold as shown in Fig. I-65. The earlier  $K^-/K^+$  ratios measured for Ni + Ni (triangles) and C + C (open squares) by the KaoS collaboration at GSI cluster near unity whereas the data from the E866 and E917 experiments at the AGS result in  $K^-/K^+$  ratios near 0.2.

The reason for this apparent discrepancy between the two data sets is not yet understood. However, a manuscript demonstrating these findings has been submitted to Phys. Rev. Lett.<sup>4</sup> A preliminary report on the pion and kaon data has been published,<sup>5</sup> and these data are the basis for the Ph.D. thesis of J. C. Dunlop, MIT.<sup>6</sup>

<sup>3</sup>L. Ahle *et al.*, Phys. Lett. **B476**, 1 (2000).

<sup>4</sup>L. Ahle *et al.*, submitted to Phys. Rev. Lett.

<sup>5</sup>W.-C. Chang *et al.*, "Advances in Nuclear Dynamics 5", Plenum Press, New York 1999, Eds. Bauer & Westfall, p. 215.

<sup>6</sup>J. C. Dunlop, Ph.D. Thesis, MIT 1999.

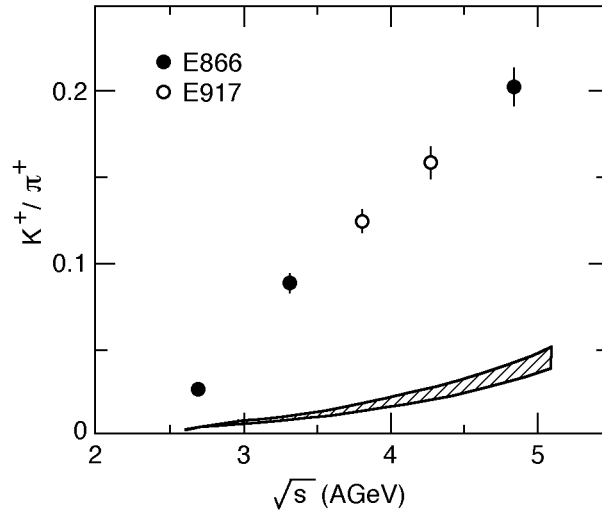


Fig. I-63. The ratio of  $dN/dy$  for  $K^+/\pi^+$  at mid-rapidity ion central Au+Au reactions as a function of the initial available energy. The data from E866 are shown as filled circles and the data from E917 are shown as open circles. The errors include a 5% systematic uncertainty. The hashed region is the  $K^+/\pi^+$  ratio from the parameterized K and  $\pi$  yields from p+p reactions (see text for details). The hashed region covers  $\pm 1\sigma$  around the p+p  $K^+/\pi^+$  ratio.

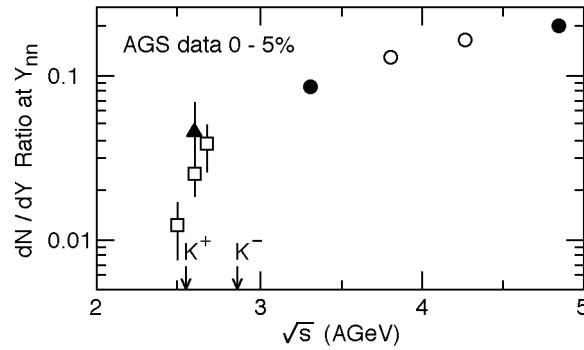


Fig. I-64. The  $K^-/K^+$  ratio as a function of  $s^{1/2}$  for central 0-5% Au+Au reactions. The data from E866 are shown as filled circles and the data from E917 are shown as open circles. Also shown are the  $K^-/K^+$  ratios measured by KaoS in Ni+Ni (triangles) and C+C (open squares)

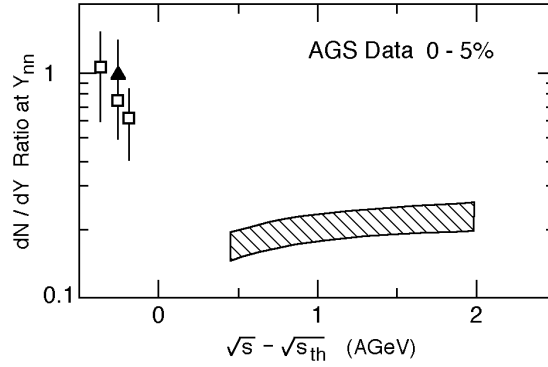


Fig. I-65. The  $K/K^+$  ratio as a function of  $s^{1/2} - s_{th}^{1/2}$ . The hashed bands represent the data as  $\pm 1\sigma$  bands calculated from the fitted  $K^+$  and  $K$  yields for central 0-5% Au+Au reactions. Also shown in both panels are the  $K/K^+$  ratios measured by KaoS in Ni+Ni (triangle) and C+C (open squares).

### $\bar{\Lambda}$ and $\bar{p}$ Production

Recently, there has been particular interest in the strange anti-baryon channel in relativistic heavy-ion collisions because it combines the QGP signatures of antimatter and strangeness. Recent results from silicon beams at the AGS and from attempts to resolve a discrepancy between AGS experiments both suggest that the  $\bar{\Lambda}$  to  $\bar{p}$  ratio may be anomalously large. In this context it is of interest that E917 can provide direct information on both the  $\bar{p}$  and  $\bar{\Lambda}$  production, the latter being obtained directly from the  $\bar{p}^+$  decay channel.

The anti-proton production was measured at a beam energy of 10.8 GeV/nucleon over four rapidity bins of  $y = 1.0-1.1$ ,  $1.1-1.2$ ,  $1.2-1.3$  and

$1.3-1.4$  and four centrality bins, namely 0%-5%, 5%-12%, 12%-23%, 23%-39%, and 39% - 77% of the total interaction cross section.

The  $\bar{\Lambda}$  production was obtained from analysis of the invariant mass spectrum of  $\bar{p}^+$  pairs. Because of lack of statistics, only two bins in centrality namely 0%-23% and 23%-77% over the rapidity region  $y = 1.0-1.4$ , were obtained. Assuming that the  $\bar{\Lambda}$  decay into  $\bar{p}^+$  is the only source of hyperon feed-down into the  $\bar{p}$  channel, we calculate the direct  $\bar{p}$  yield as  $dN(\bar{p}_{direct})/dy = dN(\bar{p}_{measured})/dy - 0.64 dN(\bar{\Lambda})/dy$ , by correcting for the 64% branching ratio of  $\bar{\Lambda}$  decays into the  $\bar{p}^+$  channel. The results of this analysis are listed in Table 2.

Table 2: This results in a  $\bar{\Lambda}$  yields and inverse slope  $T$  of  $m_t$  spectra for 0%-23% centrality over the rapidity range  $y = 1.0-1.4$  for 10.8 GeV/nucleon Au-Au collisions.

Particle	$dN/dy$	$T$ (MeV)
$\bar{\Lambda}$	$1.56 \pm 0.64 - 0.45 \times 10^{-2}$	$232^{+92}_{-51}$
$\bar{p}$	$1.50 \pm 0.06 \times 10^{-2}$	$196 \pm 11$

This results in a  $\bar{\Lambda}$  to  $\bar{p}$  production ratio of  $N(\bar{\Lambda})/N(\bar{p}_{direct}) = 3.3^{+2.0}_{-1.7}$  which is consistent with the lower limit of 2.3 reported by the E864 collaboration.<sup>7</sup> A preliminary analysis of these

data has been published,<sup>8</sup> and they were the basis for the Ph.D. thesis of George Heintzelman, MIT.<sup>9</sup>

<sup>7</sup>T. A. Armstrong *et al.*, Phys. Rev. C **59**, 2699 (1993).

<sup>8</sup>G. Heintzelman *et al.*, "Heavy Ion Physics from Bevalac to RHIC", Ed. Richard Seto, World Scientific, Singapore, 1999, pp. 205-209.

<sup>9</sup>G. Heintzelman, Ph.D. Thesis, MIT (1999).

### Phi-mesons

The possibility of in-medium modifications of the width and/or centroid of the  $\Phi$ -meson in Au - Au collisions at AGS energies was one of the original motivations for the E917 experiment. In this experiment the  $\Phi$ -meson is measured via its decay in to the  $K^+K^-$  channel by construction of an invariant mass

spectrum. The yields of  $\Phi$ 's were measured over the rapidity interval  $y = 0.9-1.4$  and the data were divided into two independent centrality bins, namely 0-23% and 23-77% of the total interaction cross section. An intermediate, but overlapping, centrality bin of 12-39% was also studied. The yields,  $dN/dy$  and inverse slopes,  $T$ , of the  $m_t$  spectra are listed in Table 3.

Table 3: Inverse slopes,  $T$ , and yields,  $dN/dy$  of the  $\Phi$ -meson as a function of the number of participants  $\langle N_p \rangle$ . (Preliminary results).

Centrality	$\langle N_p \rangle$	$T$ (MeV)	$dN/dy$
0-23%	301	$174 \pm 56$	$0.252 \pm 0.107$
12-39%	200	$229 \pm 55$	$0.129 \pm 0.027$
23-77%	104	$199 \pm 44$	$0.058 \pm 0.015$

The  $\Phi$ -yields and the ratio of  $\Phi$ -meson to  $K^-$  production at mid-rapidity is also shown in Fig. I-66(a). We note that the  $\Phi$  yield is proportional to the number of participants in the collisions,  $\langle N_p \rangle$ , although a larger than linear dependence cannot be ruled out on the basis of the data. In addition, we observe that the  $\Phi/K^-$  ratio is essentially constant with  $\langle N_p \rangle$ . Concerning the centroid and width of the  $\Phi$  mass peak in the invariant

mass spectrum, we observe good agreement with the adopted values of  $m = 1019.4 \text{ MeV}/c^2$  and  $\Gamma = 4.4 \text{ MeV}/c^2$  in p-p scattering as listed in the Particle Data Book. The analysis of the  $\Phi$  data is still in progress and additional statistical accuracy will be obtained. Preliminary results have been reported in conference proceedings,<sup>10-12</sup> and they are the basis for the Ph.D. Thesis of Hong Xiang, UC Riverside.<sup>13</sup>

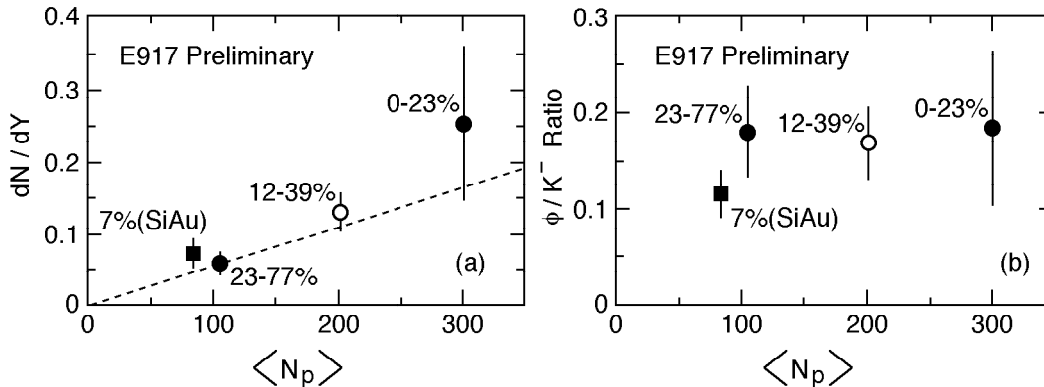


Fig. I-66. (a)  $\Phi$  yield as a function of  $\langle N_p \rangle$  and  $0.9 < y < 1.4$  from Table 3. (b)  $\Phi/K^-$  ratio as a function of  $\langle N_p \rangle$ . The ratio for Si + Au is taken from ref. 5 and is for total yields.

<sup>10</sup>W.-C. Chang *et al.*, Advances in Nuclear Dynamics 5, Plenum Press, New York 1999, Eds. Bauer and Westfall, p. 215.

<sup>11</sup>H. Xiang *et al.*, "Heavy Ion Physics from Bevelac to RHIC", Ed. Richard Seto, World Scientific, Singapore, 1999, p. 291.

<sup>12</sup>R. K. Seto *et al.*, Nucl. Phys. **A661**, 506c (1999).

<sup>13</sup>H. Xiang, Ph.D. Thesis, UC Riverside, 1999.

### Reaction Plane and Collective Flow Studies

The study of flow phenomena in relativistic heavy ion collisions provides a method for obtaining information on the collective properties of the hot and dense system produced in such reactions. These studies require accurate information on the initial trajectory of the beam particle, which was obtained from the two upstream beam vertex detectors, built at Argonne. Each detector consists of two perpendicular planes of scintillating fibers, which are read out with position sensitive photomultiplier tubes. A detailed description of this detector system and its performance in the E917 experiment has been published.<sup>14</sup> An estimate of the orientation of the reaction plane is obtained by locating the azimuthal angle of the projectile remnant after the collision using the zero degree hodoscope. We have demonstrated that the accuracy of obtaining the reaction plane in this manner is approximately  $\pm 50$  degrees.

The directed flow signal for protons and pions has been obtained using the Fourier analysis of the azimuthal distribution of particles. i.e.

$$dN/dy = A(1 + 2 v_1 \cos \phi)$$

where  $v_1$  corresponds to the first Fourier moment of the  $\phi$ -distribution.

As an example, we show in Fig. I-67(a-e) the distribution of protons for 10.8 GeV/nucleon beam energy and the 12-17% centrality bin. The rapidity bins are indicated in Fig. I-67. The solid curves represent the best fits to the data using the above expression. The resulting first Fourier moments,  $v_1$  are shown as a function of rapidity bin in panel f; the open points are reflected around mid-rapidity. We observe a clear positive flow signal for protons in this centrality bin. Preliminary analysis of the flow signals from  $^+$ , and  $^-$  both show somewhat weaker flow signals, but in the opposite direction, i.e. anti-flow.

The data analysis of the collective flow characteristics obtained in E917 is continuing and is presently being extended to the 8 GeV/nucleon beam energy.<sup>15</sup> This work will constitute the Ph.D. thesis of John-Peter Stankas, University of Maryland.<sup>16</sup>

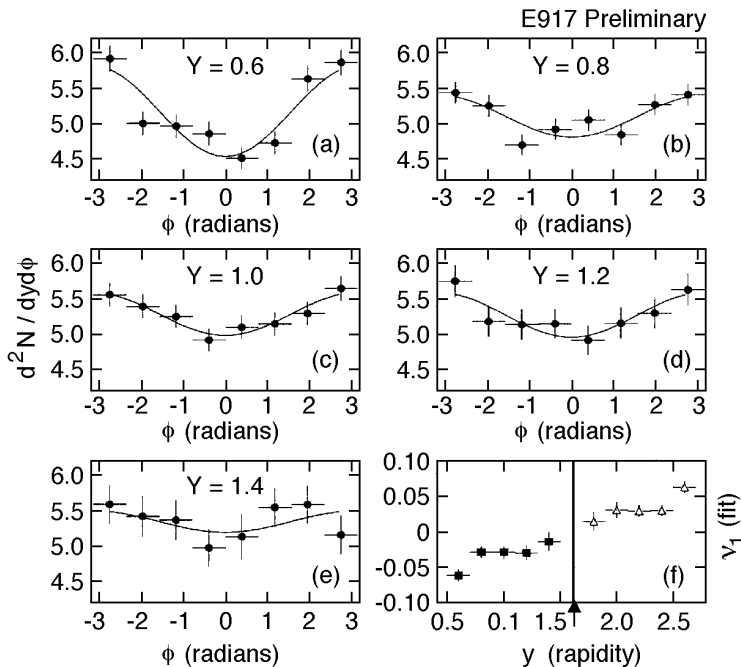


Fig. I-67. Proton directed flow signal. See text for details.

<sup>14</sup>Y. Akiiba *et al*, Phys. Rev. Lett. **76**, 2021 (1996)

<sup>15</sup>B. B. Back, R. R. Betts, A. Gillitzer, W. F. Henning, D. J. Hofman, V. Nanal, A. H. Wuosmaa, R. Ganz, B. Holzman, D. McLeod, W. R. Winns, and J. W. Epstein, Nucl. Instrum. Methods **A412**, 191 (1998)

<sup>16</sup>D. J. Hofman *et al*. "Heavy Ion Physics from Bevalac to RHIC", Ed. Richard Seto, World Scientific, Singapore, 1999, p. 98.

### Two Particle Correlations

Applying the Hanbury-Brown Twiss analysis to correlations between identical particles is an important tool for studying the size and possibly the shape of the hot fireball, from which these particles are emitted, provided certain conditions are fulfilled. We are applying this type of analysis to pairs of  $^{+}^{+}$  and  $^{-}^{-}$  pairs from Au - Au collisions at 6, 8, and 10.8 GeV/nucleon. If sufficient data are available this

analysis will also be applied to pion-pairs emitted at specific azimuthal angular bins relative to the reaction plane in order to attempt to determine possible non-spherical momenta of the fireball and/or shadowing effects of the spectators. Preliminary results from this analysis have been published in conference proceedings.<sup>17-18</sup> This work will also constitute the Ph.D. thesis for Burt Holzman, University of Illinois at Chicago.

<sup>17</sup>B. Holzman *et al.* "Advances in Nuclear Dynamics 5", Plenum Press, New York, 1999, Eds. Bauer and Westfall, p. 189.

<sup>18</sup>B. Holzman *et al.*, "Heavy Ion Physics from Bevalac to RHIC", Ed. Richard Seto, World Scientific, Singapore, 1999, p. 59.

### d.3. Heating of Nuclei with Pions and Anti-Protons (B. Back, T. Lefort,<sup>\*</sup> K. Kwiatkowski,<sup>\*</sup> W.-C. Hsi,<sup>\*</sup> L. Pienkowski,<sup>†</sup> L. Beaulieu,<sup>\*</sup> H. Breuer,<sup>‡</sup> S. Gushue,<sup>¶</sup> G. Korteling,<sup>¶</sup> R. Laforest,<sup>\*\*</sup> E. Martin,<sup>\*\*</sup> E. Ramakrishnan,<sup>\*\*</sup> L. Remsberg,<sup>§</sup> D. Rowland,<sup>\*\*</sup> A. Ruangma,<sup>\*\*</sup> V. E. Viola,<sup>\*</sup> E. Winchester,<sup>\*\*</sup> and S. J. Yennello<sup>\*\*</sup>)

Studies of the heating of heavy nuclei (Au) using antiprotons and  $^{-}$  projectiles of momentum 8 GeV/c have been carried out at the Brookhaven AGS accelerator using the Indiana Silicon Sphere 4 detector array. It is found that enhanced energy deposition is achieved with anti-protons as compared to negative

pions at this energy as illustrated in Fig. I-68. The results indicate the formation of thermal-like heavy residues with excitation energies of up to 1.5 GeV. The results are compared with the intra nuclear cascade model. Some of the results are published in Refs. 1-2.

<sup>1</sup>Lefort *et al.*, Phys. Rev. Lett. **83**, 4033 (1999).

<sup>2</sup>L. Beaulieu *et al.*, Advances in Nuclear Dynamics, 5, Eds. Bauer & Westfall, Plenum Publishers, New York, 1999, p. 1.

<sup>\*</sup>Indiana University, <sup>†</sup>Warsaw University, Poland, <sup>‡</sup>University of Maryland, <sup>§</sup>Brookhaven National Laboratory,

<sup>¶</sup>Simon Fraser University, Canada, <sup>\*\*</sup>Texas A&M University

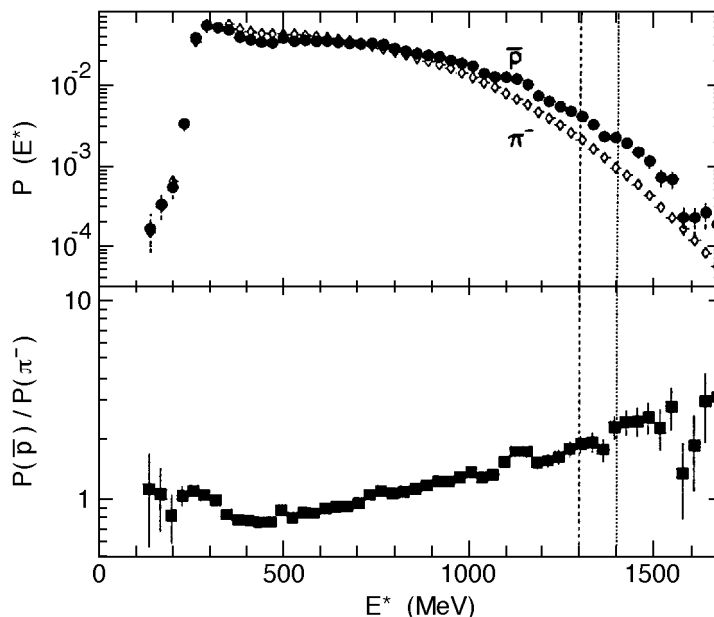


Fig. I-68. Upper panel: Excitation-energy probability distributions for reactions of 8 GeV/c  $\pi$  (diamonds) and  $\bar{p}$  (circles) with  $^{197}\text{Au}$ . Lower panel: Ratio of excitation-energy probability for  $\bar{p}$  relative to that for  $\pi$ .  $E^*$  values beyond the vertical lines (dashed:  $\pi$ ; solid:  $\bar{p}$ ) account for 1% of events.

**d.4. The PHOBOS Experiment at RHIC** (B. B. Back, N. George, A. H. Wuosmaa and the PHOBOS Collaboration - ANL, BNL, Krakow, MIT, NCU Taiwan, ORNL, U. of Rochester, UIC, and U. of Maryland)

**Overview**

At RHIC, heavy ions will collide at center of mass energies an order of magnitude higher than have previously been available anywhere. There, it is expected that a baryon-free region of extremely high energy density will remain after the two colliding nuclei have passed through each other. It is believed that this situation will be more than sufficient to create a system of deconfined quarks and gluons - the "Quark Gluon Plasma". After formation, the plasma should expand and cool before passing into the normal hadronic phase which in turn further expands until the hadrons cease to interact with each other ("freezeout"). The questions are then what are the direct probes and signatures of the plasma phase, and what identifiable traces of the quark-gluon phase remain in the observed hadronic final state? The PHOBOS experiment seeks to address these questions.

The PHOBOS experiment focuses on measurements of hadronic observables for a very large sample of events. The PHOBOS apparatus consists of a 4 multiplicity detector and two multi-particle spectrometers capable of measuring and identifying particles with very low transverse momenta. The multiplicity detector will provide event-by-event charged-particle multiplicity distributions, which can be used to find interesting events for study in more detail using the spectrometers. The multiplicity distributions are interesting on their own, and contain information on fluctuations and correlations, which relate to some of the proposed signatures of the plasma.

An overall view of the PHOBOS apparatus is shown in Fig. I-69; several different components are identified. The fabrication of the multiplicity and Vertex detectors is the responsibility of the groups at Argonne and UIC. Together, these systems contain over 22000 channels of silicon pad detector.

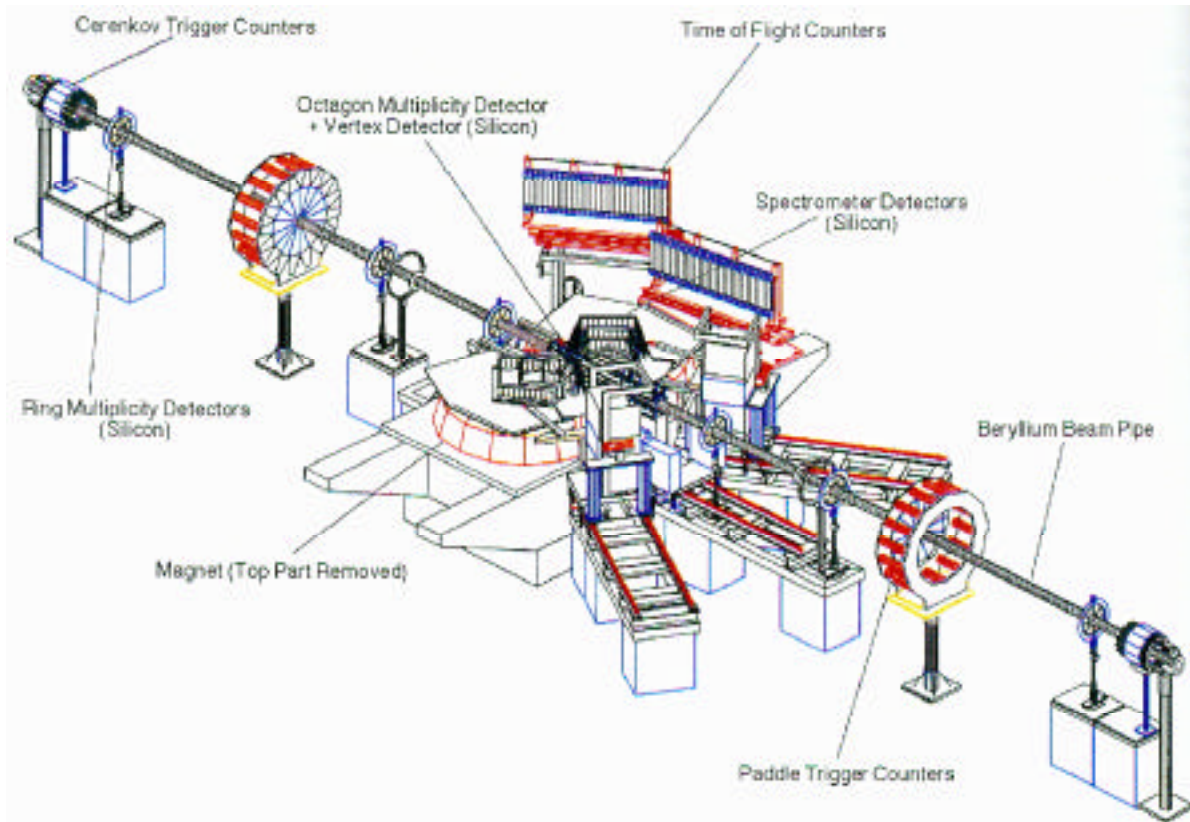


*Fig. I-69. Overview of the PHOBOS experimental setup. The top half of the spectrometer magnet has been removed for clarity.*

The Multiplicity detector will provide event-by-event information on the charged particle multiplicity distributions over  $\pm 5$  units of pseudo-rapidity, with complete azimuthal coverage. For central Au + Au collisions at RHIC, the total charged particle multiplicity in this pseudo-rapidity range is expected to be of order 6000 or greater. The multiplicity measurement is made using a centrally located, 11000 channel "Octagon" array of silicon pads supplemented with six 512 channel "Ring" counters placed up and down the beam pipe. These detectors will measure the energy deposited as a function of angle with respect to the collision vertex. Multiple hits can be handled in an average way by dividing the measured energy by the average expectation for a single charged particle at that point in the detector. Monte Carlo studies have shown that the charged particle multiplicity distributions for central Au + Au collisions can be reconstructed with systematic errors small compared to normal Poisson fluctuations.

The Vertex detector is designed to locate the position of the interaction vertex on an event by event basis. It is composed of two pairs of planes of silicon pad detectors, each plane segmented into 2048 channels so that the occupancy is low. Particles emitted from the collision vertex can be tracked by combining pairs of hits on the inner and outer Vertex planes such that the position of the reconstructed interaction point can be determined to a precision of better than  $300 \mu\text{m}$ . Vertices may be reconstructed over the entire range of the RHIC collision diamond, corresponding to  $\pm 20$  cm about the center of the intersection region.

In the past 12 months, the PHOBOS experiment has undergone a tremendous amount of progress, and at this writing, all of the detector components required for the experiment for the first years running are complete. The following sections describe the status of elements which are the primary responsibility of the ANL/UIC collaboration, i.e. the multiplicity and vertex detectors.

### Assembly and Testing Status

The assembly and quality control testing procedures of the detector modules that make up the Multiplicity and Vertex detectors in PHOBOS are carried out at the University of Illinois at Chicago, ANL, and the Silicon Detector Facility at Fermi National Accelerator Laboratory. The hybrids that carry the front-end electronics chips for each detector module are initially fabricated under the supervision of the MIT electronics laboratory. These circuits, which consist of either 128, or 64, channels of charge-sensitive preamplifier and shaping elements, are mounted on the hybrids. Micro-wire bonding of electronics connections between the preamplifier chip and the hybrid was carried out at FNAL, and the units are subsequently electronically tested at ANL. Those that pass the initial quality control evaluation are returned to UIC, where the silicon sensors are affixed to them. The now fully-fledged detector modules are returned to FNAL, where the individual channel connections are made by additional wire bonding. The resulting detector modules return to ANL where they are further evaluated, both with electronic testing, as well as with

radioactive sources. Those modules that pass all quality control evaluations are then used for installation in the experiment.

At present, all silicon modules needed for the multiplicity and vertex detector arrays are complete. This complement includes 128 Multiplicity Octagon and 50 Multiplicity Ring modules, and 21 Vertex detector modules, containing over 33000 channels, all of which have been subjected to the various acceptance tests. These have been delivered to BNL.

### Installation and Testing of the Complete PHOBOS Detector

At the end of 1999, the modules that make up the Year 1 physics detector for PHOBOS were mounted on their respective frames. The assembled mid-rapidity frame carrying 94 Octagon, and 12 Vertex detectors, and the six high-rapidity multiplicity arrays each carrying 8 ring detector modules, were assembled at BNL. Figure I-70 shows the assembled octagon, and two ring detectors, in the assembly laboratory at BNL.

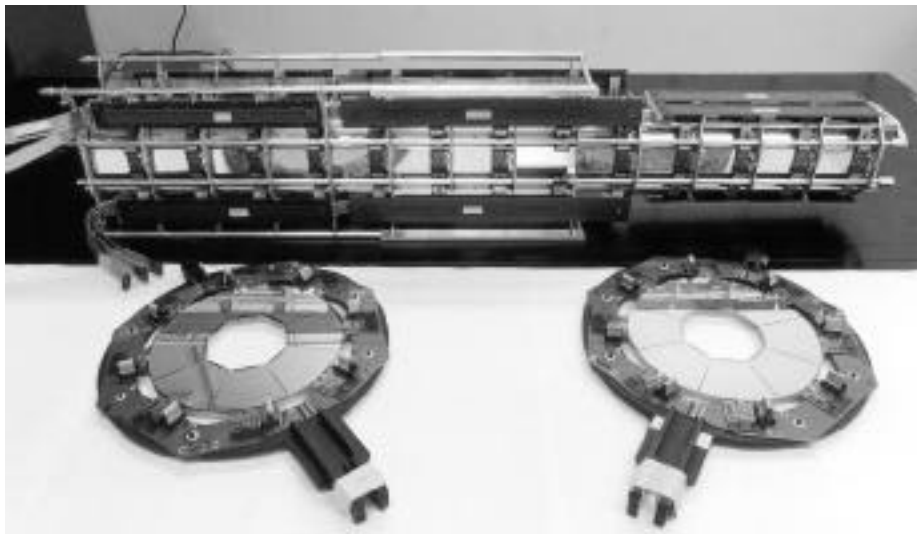


*Fig. I-70. Assembled Octagon and Ring detectors for PHOBOS in the assembly laboratory at Brookhaven National Laboratory.*

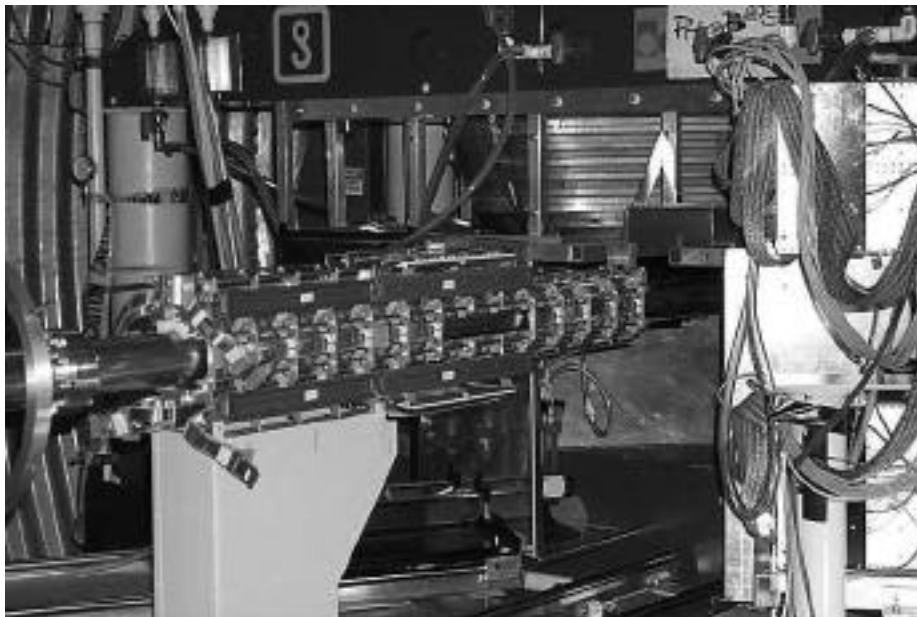


*Fig. I-71. Central multiplicity and vertex detector assembly installed in the RHIC tunnel around the beam pipe, prior to insertion into the central magnet gap.*

After the detector modules were mounted on their respective frames, these frames were installed in the experimental hall in the RHIC tunnel. Figure I-72 shows the loaded octagon frame in position around the beam pipe, prior to insertion into the central magnet gap. Figure I-72 shows one of the six ring arrays, as well as one of the two high-Cerenkov trigger detector arrays, also in position around the beam pipe. With this installation, the construction of PHOBOS is essentially complete, signifying a major milestone for the PHOBOS experiment.

The stability and performance of the system was evaluated over a 4-day period in early 2000. Detector leakage currents, pedestals, noise and gain for each of the approximately 70000 channels in the full

experiment were monitored for stability, and also as a test of the full data acquisition system. The stability of the full system was excellent, with gain and pedestal variations of order 1% or less. The temperature and leakage current stability was also excellent, owing to the performance of the chilled water cooling system that keeps all silicon detector elements of the experiment at a constant temperature. Subsequent to this test, the full complement of the detectors to be used in the Year-1 physics run was removed, and replaced with a limited subset of silicon modules. This was done in order to protect the silicon and front-end electronics chips from the harsh radiation conditions expected during the tuning and commissioning stages of beam development for Year-1 physics running (see below).

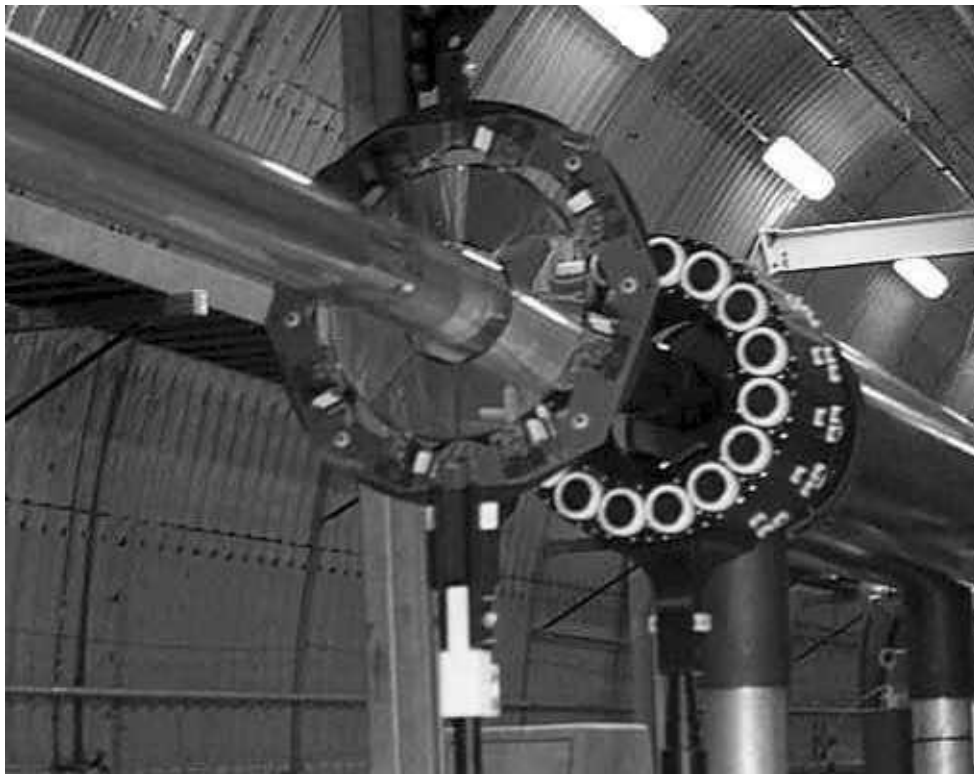


*Fig. I-72. One of six multiplicity ring detectors, and one of two high- $\eta$  trigger detectors installed around the RHIC beam pipe.*

#### The Summer Engineering Run and First Beam in RHIC

During the summer of 1999, the first Au beams were injected and circulated in the RHIC rings. The purpose of this running period was to commission the accelerator, to understand the collider optics, and to provide the experiments with the first possibility to obtain data with injected beams. During this period Au beams from the BNL AGS were injected with an energy of 10.8 GeV/nucleon, and were circulated in the two RHIC rings individually. In one of the two rings (the “Blue” ring), reasonable tuning conditions were achieved and stable orbits with lifetimes of the order of 1000s of turns were obtained. For the second (“Yellow”) ring, somewhat poorer results, with beam lifetimes of order only 100s of turns, were obtained before termination of the Engineering Run. In addition to evaluation of the collider optics, the RF system was exercised and capture was achieved (a necessity for long beam lifetimes), and some acceleration was performed for beams in the Blue ring. At no time were

beams present simultaneously in the two rings, and consequently no collisions were produced. Despite this, there were events from the scattering of the Au ions from residual gas, as well as from beamline components that produced particles that could be detected in the experiments.

PHOBOS employed a subset of its full physics detectors for data taking during the engineering run. A single “ladder” of octagon multiplicity modules, two vertex detectors, and a component of trigger and plastic-scintillator detectors, were installed in the RHIC tunnel. These were read out with a prototype version of the PHOBOS data acquisition system. The trigger detectors were capable of firing either on beam-induced, or Cosmic-ray particles. Figure I-73 shows a histogram of the energy deposited by cosmic-ray particles passing through the octagon detectors. A clear minimum-ionizing peak is observed at an energy of approximately 100 keV deposited in the detector.

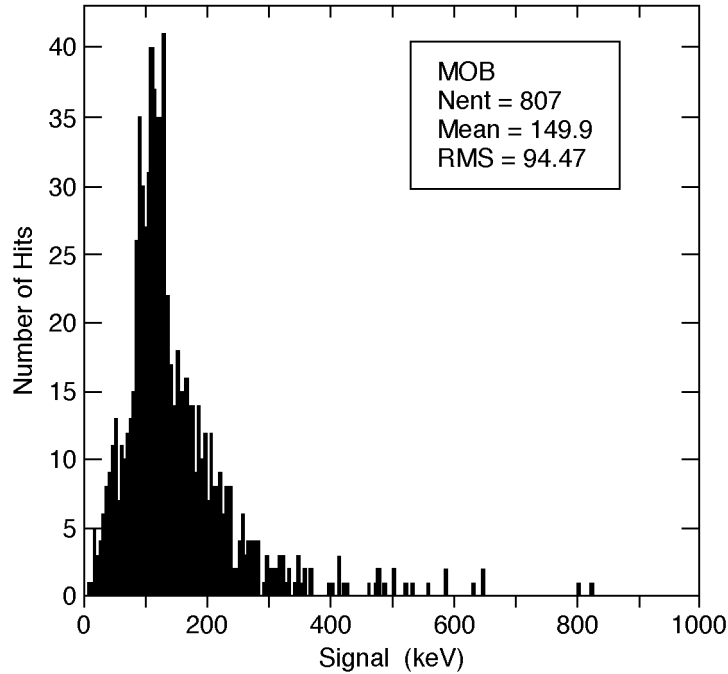


Fig. I-73. Histogram of energy loss in the Engineering run octagon detector. The peak corresponding to minimum ionizing particles is at an energy of 100 keV.

Figures I-74 and I-75 show spectra of energy deposited in the octagon and vertex detectors from particles produced by interactions of the Au beam with either residual gas or components of the RHIC beamline. The differences in the widths of the two minimum-ionizing

peaks arises from the fact that most of the beam induced particles are produced moving nearly parallel to the beam, and intersect the silicon detectors at very small angles. The vertex detectors possess much

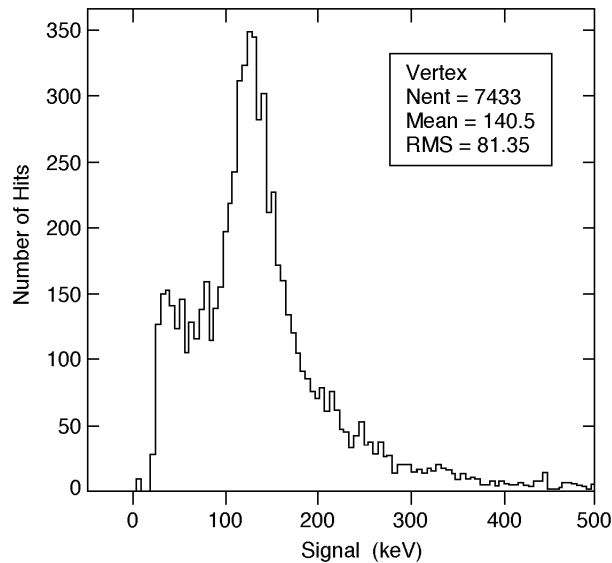


Fig. I-74. Energy-loss spectrum for beam induced particles detected in a Vertex sensor.

smaller pads than those in the octagon sensors, and therefore the particles traverse a smaller volume of silicon, and deposit a correspondingly smaller amount of energy in the vertex pads, as compared to the octagon.

On occasion, there would be events that produced very large numbers of particles resulting in large observed energy deposition signals in all channels of the silicon detectors. These so-called “blast” events, presumably arising from an entire bunch of Au ions impacting a beamline magnet or other component, had a detrimental

effect on the silicon performance, and often resulted in a phenomenon known as “CMOS latchup”. Under this condition, the front-end electronics chips fail to work properly, although generally this failure condition was recoverable. A consequence of this observation was that the front-end control electronics was modified to identify this condition and to protect the front-end electronics chips from it. In addition, the decision was made to postpone installation of the full detector system for the initial physics run until stable beam conditions were achieved in the RHIC rings.

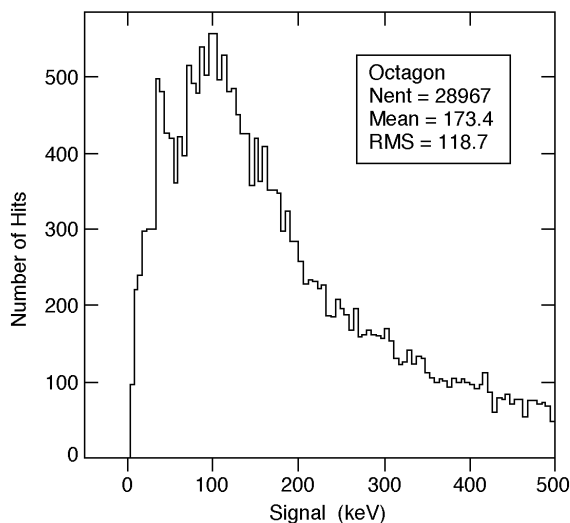


Fig. I-75. Energy-loss spectrum for beam induced particles detected in an Octagon sensor.

#### Multiplicity Reconstruction and Early Physics Analyses

In preparation for the first data from PHOBOS, much consideration is being given to the first data analyses, and to the extraction of physics results. Chief among these are the values of the rapidity density  $dN/d$  at mid-rapidity, and the multiplicity distribution for charged particles as a whole. For the important quantity  $dN/d|_{=0}$ , data from the central region of the octagon, as well as from the vertex detectors and the forward spectrometer planes, are all important. The chief uncertainties in any analysis of charged-particle multiplicity in PHOBOS arise from both the contributions of secondary particles, and from the transformation of measured energy-deposition signals to the number of particle tracks within a given pad in the silicon detectors. Near mid-rapidity, the vertex detectors and most highly segmented spectrometer planes are able to resolve individual particle tracks. A comparison of these measurements to the multiplicity determined from the energy deposited in the larger

octagon detector pads constitutes a valuable crosscheck for the multiplicity determination. Analyses of Monte-Carlo data designed to study this problem are currently underway.

Beyond mid-rapidity, the octagon is the primary tool for measuring charged-particle multiplicity, although these determinations will be compared with, and augmented by, other measurements from the trigger counters and zero-degree calorimeters in order to correlate the multiplicity data with other experimental parameters, such as impact parameter. Away from mid-rapidity, it is expected that the backgrounds from secondary particle production will be considerable. One task of the early data analysis will be to understand these backgrounds and to determine how they affect the reconstructed multiplicity distributions. Once these issues are resolved, the multiplicity data will be used to confront the predictions of the various event generators, to identify possibly interesting events with large multiplicities, and to search for unusual fluctuations in

$dN/d$  as possible evidence of new physics. An example of the kind of data that may be obtained with the multiplicity detector array appears in Fig. I-76, which shows typical multiplicity distributions for central events obtained from the event generator HIJING. Shown in Fig. I-76 are the distribution from a single event as predicted by HIJING, that same

distribution as reconstructed by PHOBOS, and the average multiplicity distribution from 200 such events. Current indications are that the systematic uncertainties introduced by the multiplicity reconstruction procedure will be comparable to, or smaller than, the statistical uncertainties inherent in the data.

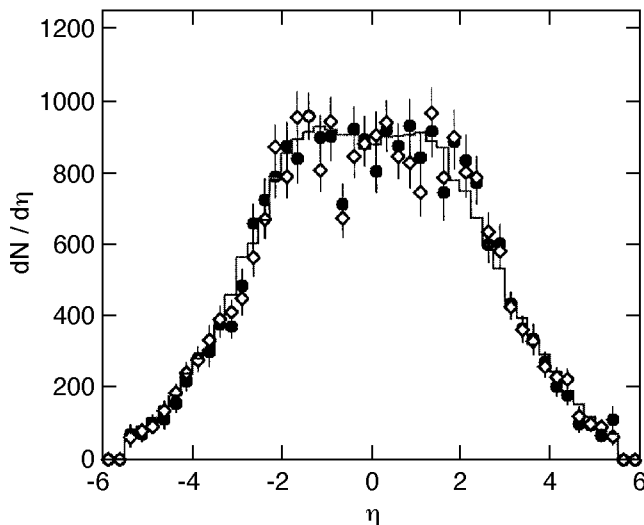


Fig. I-76. Multiplicity distribution from one HIJING event (solid symbols), the same event reconstructed (open symbols) and the average of 200 HIJING events (histogram).

#### Status and Schedule

RHIC is presently scheduled to begin injection and tuning of Au beams for the Year-1 physics run in April-May 2000. As discussed above, while the PHOBOS hardware is complete, for the initial beam tune of RHIC, the full PHOBOS apparatus will not be present in the tunnel. Instead, a subset of detectors including one ladder of octagon sensors, 1/4 of the Vertex detector, 4 planes of tracking spectrometer, and trigger

detectors will be installed. The initial beam tune is expected to take of order 1 month, from injection to tuning for collisions. Following this tuning period, the commissioning setup will be removed from the tunnel, and replaced with the full apparatus. As previously noted, this installation is projected to require no more than approximately two weeks. Data taking with the full physics setup will continue until the conclusion of the Year-1 run, at the end of August 2000.